Polarizabilities (α) of Dendritic Molecular Aggregates: Visualization of Intermolecular-Interaction and Damping Effects on α

Masayoshi Nakano,* Masahiro Takahata, Harunori Fujita, Shinji Kiribayashi, and Kizashi Yamaguchi

Department of Chemistry, Graduate School of Science, Osaka University, Toyonaka, Osaka 560-0043, Japan

Received: December 31, 2000; In Final Form: March 20, 2001

We investigate the intermolecular-interaction and damping (among exciton states) effects on the polarizabilities (α) for molecular aggregates with different sizes of planar dendritic, i.e., Bethe-lattice (or Cayley-tree), structures by elucidating the spatial contribution of one-exciton generation to α. The molecular aggregate is treated in the one-exciton model, including the dipole−dipole interaction. The off-resonant α of the molecular aggregate is calculated by the numerical Liouville approach, including the damping effects. The signs of the contribution of intermolecular-interaction (positive) and damping (negative) effects to α are found to be opposite with each other. The magnitude of these effects on α indicates a nonlinear enhancement as the number of monomers increases. These effects on α for the fractal-structured dendritic aggregates are also found to provide distinct spatial contributions for different generations of the dendritic structure in contrast to the case of a non-fractal-structured dendritic aggregate.

1. Introduction

Recently, dendrimeric supramolecules with fractal antenna structures have attracted a great deal of attention because of their remarkable light-harvesting ability.[1−12] These molecular systems have a large number of terminal groups originating in a focal point (core) with at least one branch at each repeat unit. It is predicted that there is an efficient directional energy transfer from the periphery to the core. Such excitation energy cascades to the core are known to be caused by the exciton migration in the fractal antenna structure, which provides ordered energy states. On the other hand, molecular aggregate systems with dendritic structures are also known to exhibit similar ordered energy states and directional energy transfer.[13] Although the first-order optical processes, i.e., absorption and emission of light, for these systems have been investigated actively, the optical response processes, e.g., (hyper)polarization, have not been elucidated well. In this study, therefore, we focus on the features of polarizabilities α for several sizes of dendritic molecular aggregates (with planar structures), in which monomers (chromophores) are assumed to be dipole units (two-state molecular models coupled with each other by dipole−dipole interaction) arranged as modeled after the Bethe-lattice (or Cayley-tree) type structures.[10−12] These dendritic aggregate models are modeled after phenylacetylene dendrimers, and the decoupling of π-conjugation at branching points (benzene rings) are realized by increasing intermolecular distance between neighboring units through branching points. As mentioned above, these aggregate models can reproduce some primary features (multistep exciton states and decoupling at branching points) of exciton states for dendrimers. On the other hand, because the effects of the dipole−dipole interaction are weaker than those of the π-electronic conjugation, the size dependences of α for dendritic aggregates are predicted to be fairly smaller than those for dendrimers. However, the size dependency of the intermolecular-interaction effects in dendritic aggregates and their spatial contribution to α is expected to more clearly reflect the effects of the fractal structure. Considering the intensity of the π conjugation in dendrimers, similar features are expected to be observed more remarkably in α for dendrimers.

We use a conventional one-exciton molecular aggregate model constructed from chromophore dipole units, which are coupled with each other by the dipole−dipole interaction. The energy states and transition moments for the model aggregate are calculated by diagonalizing the model Hamiltonian matrix. Using this aggregate-state model, the time evolution of the density matrix is calculated in a numerically exact manner, i.e., numerical Liouville approach (NLA).[14] Because it is recently pointed out that the damping effects in exciton states are important for the exciton migration from the periphery to the core of these dendritic systems,[15] we here examine two cases of models with and without damping terms. The α values in the off-resonant region are calculated using our definition of nonperturbative α. The nonperturbative approach has an advantage of easily treating such damping effects originating in exciton−phonon coupling. Furthermore, under the (near) resonant condition, the nonperturbative approach is essential for treating response properties. As mentioned above, the exciton migration dynamics under the (near)resonant condition are a recent topical subject, so that we present our nonperturbative approach, which is applicable to the calculation of α both in off- and on-resonant regions, though this approach is not necessary for the present case with weak off-resonant fields. To elucidate the feature of α, we develop a visualization method of the spatial contribution of virtual one-exciton generation to α. Using this plot, we investigate the intermolecular-interaction and damping effects on the spatial contribution of one-exciton generation to α for different-size dendritic aggregates and elucidate the structure−property relation in α of dendritic systems with a fractal-dimensional structure.

* To whom correspondence should be addressed. E-mail: mnaka@chem.sci.osaka-u.ac.jp.

10.1021/jp004593b CCC: $20.00
Published on Web 05/10/2001

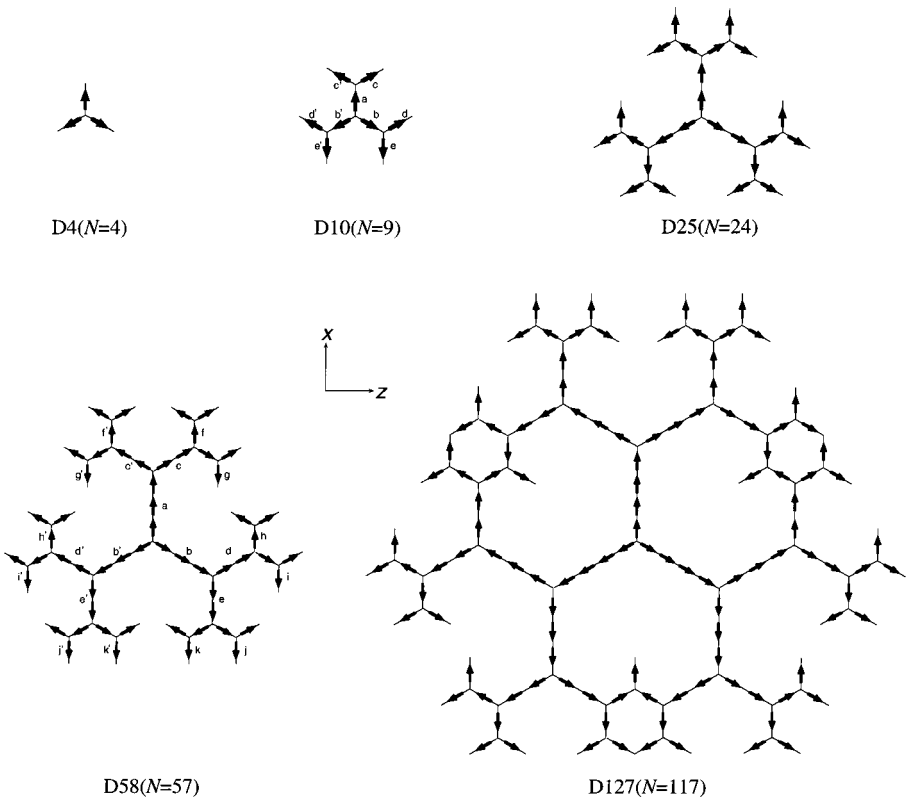

Figure 1. Structures of dendritic molecular aggregates (D4, D10, D25, D58, and D127) which mimic skeletons of phenylacetylene dendrimers.[10−12] *N* represents the number of monomers. Each two-state monomer dipole unit (with transition energy $E_{21} = 38\,000$ cm^{-1} and transition moment $\mu_{21} = 10$D) is represented by an arrow. The intermolecular distance in linear legs and the angle between neighboring linear legs at all branching-points are assumed to be 15 au and 120°, respectively.

2. Methodology

2.1. Model Hamiltonian of Molecular Aggregates. We consider dendritic molecular aggregates (Figure 1) composed of two-state monomers (chromophores). The *k*th monomer possesses a transition energy, $E^k_{21}(\equiv E^k_2 - E^k_1)$, and a transition moment, $\boldsymbol{\mu}^k_{12}$. The monomer is approximated to be a dipole. This approximation is considered to be acceptable if the intermolecular distance (R_{kl}) is larger than the size of a monomer. For two dipoles *k* and *l*, the angle between a dipole $k(l)$ and a line drawn from the dipole site *k* to *l* is $\theta_{k_l}(\theta_{l_k})$. The Hamiltonian for the aggregate model is written by

$$H_{\mathrm{agg}} = \sum_{k}^{N}\sum_{i_k}^{2} E^{k}_{i_k} a^{+}_{i_k} a_{i_k} + \frac{1}{4\pi\epsilon_0}\sum_{k<l}^{N}\sum_{\substack{i_k,i'_k \\ i_l,i'_l}}^{2} \mu^{k}_{i_k i'_k}\mu^{l}_{i_l i'_l}[(\cos(\theta_{k_l} - \theta_{l_k}) - 3\cos\theta_{k_l}\cos\theta_{l_k})/R^3_{kl}]a^{+}_{i_k} a_{i'_k} a^{+}_{i_l} a_{i'_l} \quad (1)$$

where the first and the second terms represent a noninteracting Hamiltonian and a dipole−dipole interaction. *N* represents the number of dipole units. $E^k_{i_k}$ is an energy of the state i_k for monomer *k*, and $\mu^k_{i_k i'_k}$ is a magnitude of a transition matrix element between states i_k and i'_k for monomer *k*. The $a^{+}_{i_k}$ and a_{i_k} represent respectively the creation and annihilation operators for the i_k state of monomer *k*. The matrix elements of H_{agg} in the basis for the aggregate $\{|\varphi^1_{i_1}\varphi^2_{i_2}\cdots\varphi^N_{i_N}\rangle\}$ (*N* is the number of monomers), which is constructed from a direct product of a state vector for each monomer $\{|\varphi^k_{i_k}\rangle\}$, are presented in our previous paper.[13] By diagonalizing the Hamiltonian matrix *H* (eq 1), we can obtain eigenenergies $\{E^{\mathrm{agg}}_l\}$ and eigenstates $\{|\psi^{\mathrm{agg}}_l\rangle\}$ ($l = 1,..., M$), where *M* is the size of the basis used. *M* is $N + 1$ in the present study because we consider a one-exciton model. The transition dipole matrix element ($\mu^{\mathrm{agg}}_{ll'}$) in the direction of applied field for this new state model is also calculated.[13] It is noted that the transition moments between the ground and one-exciton states, and those between one- and two-exciton states, only exist in the present model.

2.2. Density Matrix Formalism for Molecular Aggregate under Time-Dependent Electric Field. We here briefly explain our nonperturbative calculation approach, i.e., NLA.[14] The time evolution of a molecular aggregate model is described by the following density matrix formalism:[14]

$$i\hbar\frac{\partial}{\partial t}\rho(t) = [H(t),\rho(t)] - i\Gamma\rho(t) \quad (2)$$

where $\rho(t)$ indicates the total molecular density matrix and the second term on the right-hand side of eq 2 represents the damping processes in the Markoff approximation. The total Hamiltonian $H(t)$ is expressed by the sum of the aggregate Hamiltonian, H_{agg}, and aggregate-field interaction, $V(t)$

$$H(t) = H_{\mathrm{agg}} + V(t) = \sum_{l=1}^{M} E^{\mathrm{agg}}_l b^{+}_l b_l - \sum_{l,l'=1}^{M}\mu^{\mathrm{agg}}_{ll'}(F\cos\omega t)b^{+}_l b_{l'} \quad (3)$$

where *F* is an external field amplitude in the direction of *x* because the incident field is assumed to be a plane wave with frequency ω and wave vector $\boldsymbol{k}$ travelling perpendicular to the molecular plane and the polarization vector is parallel to the *x* axis. b^{+}_l and b_l represent respectively the creation and an-

nihilation operators for the l state of the aggregate state model obtained in section 2.1. The matrix representation of eq 2 is expressed as

$$\dot{\rho}_{ll'}(t) = -i(1-\delta_{ll'})E^{\mathrm{agg}}_{ll'}\rho_{ll'}(t) - i\sum_{m}^{M}(V_{lm}(t)\rho_{ml'}(t) - \rho_{lm}(t)V_{ml'}(t)) - (\Gamma\rho(t))_{ll'} \quad (4)$$

where $V_{ll'}(t) = -\mu^{\mathrm{agg}}_{ll'}(F\cos\omega t)$.

The damping term $-(\Gamma\rho(t))_{ll'}$ in eq 4 can be considered as the following two types of mechanisms:[14]

$$-(\Gamma\rho(t))_{ll} = -\Gamma_{ll}\rho_{ll}(t) + \sum_{m\neq l}^{M}\gamma_{ml}\rho_{mm}(t) \quad (5)$$

and

$$-(\Gamma\rho(t))_{ll'} = -\Gamma_{ll'}\rho_{ll'}(t) \quad (6)$$

Equations 5 and 6 describe the population and coherent-damping mechanisms, respectively. $\gamma_{ll'}(\neq\gamma_{l'l})$ represents a feeding parameter. The off-diagonal damping parameter is expressed as

$$\Gamma_{ll'} = \frac{1}{2}(\Gamma_{ll} + \Gamma_{l'l'}) + \Gamma'_{ll'} \quad (7)$$

and

$$\Gamma_{ll'} = \Gamma_{l'l} \quad (8)$$

where Γ'_{ij} is the pure dephasing factor. In this study, because we assume a closed system, the factor $\gamma_{ll'}$ is related to the decay rate as

$$\Gamma_{ii} = \sum_{l\neq i}^{M}\gamma_{il} \quad (9)$$

We perform a numerically exact calculation to solve eq 4 by the fourth-order Runge−Kutta method. The density matrix representation in the aggregate basis $\{|\varphi^1_{i_1}\varphi^2_{i_2}\cdots\varphi^N_{i_N}\rangle\}$ at time t is calculated by

$$\rho_{i_1,i_2,\ldots,i_N;i'_1,i'_2,\ldots,i'_N}(t) = \sum_{l,l'=1}^{M}\langle\varphi^1_{j_1}\cdots\varphi^N_{j_N}|\psi^{\mathrm{agg}}_{l}\rangle\,\rho_{ll'}(t)\,\langle\psi^{\mathrm{agg}}_{l'}|\varphi^1_{j'_i}\cdots\varphi^N_{j'_N}\rangle \quad (10)$$

where $\rho_{ll'}(t)$ is calculated by eq 4. Using this density matrix, the polarization $\rho(t)$ is calculated by

$$p(t) = \sum_{\substack{i_1,i_2,\ldots,i_N,\\ i'_1,i'_2,\ldots,i'_N}}^{M}\mu_{i_1,i_2,\ldots i_N;i'_1,i'_2,\ldots i'_N}\rho_{i'_1,i'_2,\ldots,i'_N;i_1,i_2,\ldots,i_N}(t) \quad (11)$$

Here, the transition matrix element $\mu_{i_1,i_2,\ldots i_N;i'_1,i'_2,\ldots i'_N}$ is represented by

$$\mu_{i_1,i_2,\ldots i_N;i'_1,i'_2,\ldots i'_N} = \langle\varphi^1_{i_1}\cdots\varphi^N_{i_N}|\sum_{l=1}^{N}\mu'^{l}|\varphi^1_{i'_1}\cdots\varphi^N_{i'_N}\rangle = \sum_{l=1}^{N}\mu^{\prime l}_{i_l i'_l}\Big(\prod_{n\neq l}^{N}\delta_{i_n i'_n}\Big) \quad (12)$$

where $\mu^{\prime l}_{i_l i'_l}$ represents a transition dipole matrix element (in the direction of polarization vector of applied field) between i_l and i'_l of monomer l.

2.3. Calculation Method of Polarizability and Its Partition into the Exciton Generation. We briefly explain our calculation method of α in the NLA.[14] The polarization $p(t)$ is transformed to $p(\omega)$ in the frequency domain by using the discrete Fourier transformation. Using the external field amplitude $\epsilon(\omega)$ ($= F/2$) and the polarization $p(\omega)$, the nonperturbative $\alpha(-\omega;\omega)$ ($\equiv \alpha_{xx}(-\omega;\omega)$) for a molecular aggregate is calculated by

$$\alpha(-\omega;\omega) = \frac{p(\omega)}{\epsilon(\omega)} \quad (13)$$

For weak fields, this quantity coincides with the conventional perturbative $\alpha(-\omega;\omega)$. Although in the present case the intensity-dependent phenomena[14] described by eq 13 seem not to be observed, we apply this nonperturbative approach to the calculation and analysis of α because of its advantages mentioned in section 1. From eqs 11 and 13, the $\alpha(-\omega;\omega)$ is also expressed as

$$\alpha(-\omega;\omega) = \sum_{a>b}^{M}\alpha_{a-b} = \sum_{a>b}^{M}\frac{2\mu_{ab}\rho^{\mathrm{real}}_{ba}(\omega)}{\epsilon(\omega)} \quad (14)$$

where a and b indicate the aggregate basis $\{|\varphi^1_{i_1}\cdots\varphi^N_{i_N}\rangle\}$ and $\rho^{\mathrm{real}}_{ba}(\omega)$ is a Fourier component of the real part of density matrix element ($\rho^{\mathrm{real}}_{ba}(t)$) in the aggregate basis. Equation 14 indicates that the total α can be partitioned into the virtual excitation contribution (α_{a-b}) between bases a and b. In the one-exciton case, either a or b is $|11\ldots1\rangle$ (1. the ground state of monomer), so that we can elucidate the spatial contribution of one-exciton generation to α by showing the one-exciton distribution, e.g., $|121\ldots1\rangle$ (2. the excited state of monomer).

3. Results and Discussion

3.1. One-Exciton States and Their Spatial Contribution to α of Dendritic Aggregate Models. The dendritic molecular aggregate models (D4, D10, D25, D58, and D127) shown in Figure 1 involve all of the same dipole units. The transition energy and transition moment of the dipole unit (monomer) are assumed to be 38 000 cm^{-1} and 10 D, respectively. It is noted that the magnitude of these parameters does not affect the qualitative results for the relative size dependency of intermolecular-interaction and damping effects on α and their spatial contributions to α. These aggregate models possess slight intermolecular interactions between adjacent legs at the branching points because their intermolecular distance ($15\sqrt{3}$ a.u.) is larger than that (15 au) in the same leg regions. It is noted that such considerable decreases in the intermolecular interactions at the branching points are similar to the situation in real phenylacetylene dendrimers, in which the meta-branching points destroy the π-electronic conjugation between adjacent linear legs.[12] The one-exciton states l ($l = 2,\ldots, M$) and the magnitude of transition moments between the ground and the one-exciton states for these aggregate models are shown in Figure 2. There are found to be explicit multistep energy states (with significant transition moments) for these dendritic aggregates (except for a small dendritic aggregate (D4)) in contrast to the case of linear aggregates which possess almost only a one-exciton energy state with a significant transition moment.[12,13] It is also found that the number of such multistep energy states and the energy width of their distribution increase with the increase in the dendritic-aggregate size, corresponding to the number of generations

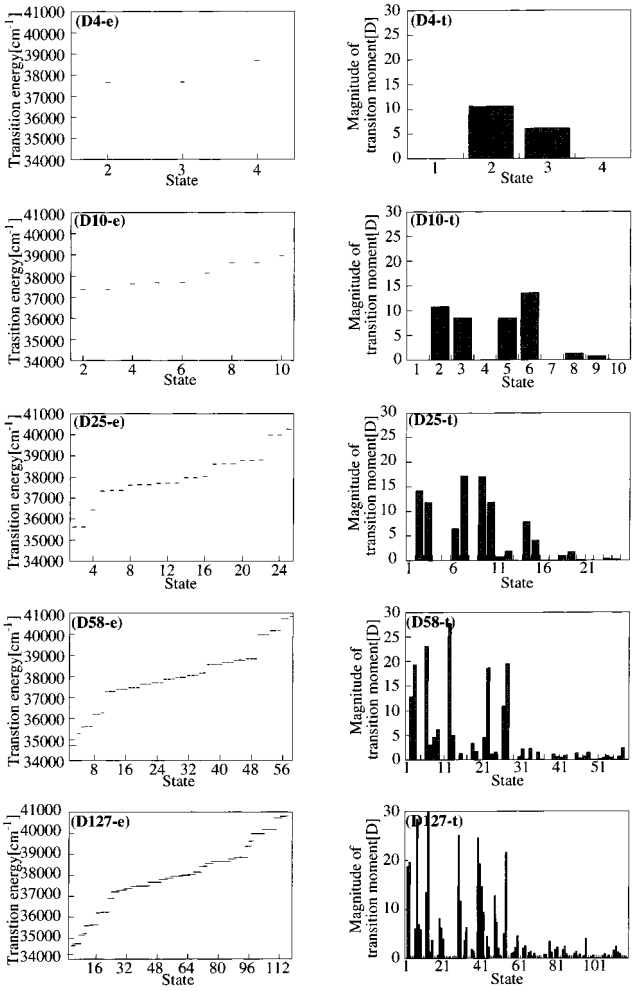

Figure 2. Calculated one-exciton state energies E_{l1}^{agg} [cm^{-1}] and the magnitude of transition moments μ_{l1}^{agg} [D] between the ground (1) and one-exciton (l) states of the dendritic molecular aggregates shown in Figure 1.

involved in the dendritic structure. These multistep energy structures can be explained by the *J*- and *H*-aggregate-type interactions[16,17] involved in the dendritic (fractal antenna) structure and are known to be important for the exciton migration from the periphery to the core.[13]

Because the damping effects in one-exciton states are found to be essential for the exciton migration from the periphery to the core of dendrimer,[15] we consider the damping terms in eq 2. The factor γ_{il} in eq 5 is determined by an energy-dependent relation: $\gamma_{il} = f(E_i^{agg} - E_l^{agg})$ ($f = 0.1$, i ($>l$) is a one-exciton state). This indicates that the population of higher energy states decreases faster and damps into the lower energy states. The external single-mode laser with 100 MW/cm^2 has a frequency (3000 cm^{-1}), which is sufficiently off-resonant with respect to one-exciton states. It is noted from the perturbational formula (eq 15) that the off-resonant α can be qualitatively well described in the one-exciton model. The division number of the one optical cycle of the external field used in the numerical calculation is 80, and the α is calculated by using 100 optical cycles after an initial nonstationary time evolution (2000 cycles). In general, the feature of off-resonant α can be explained by the following perturbational formula:

$$\alpha(-\omega;\omega) = 2\sum_{l=2}(\mu_{1l})^2 \frac{E_{l1}}{(E_{l1}^2 - (\hbar\omega)^2)} \qquad (15)$$

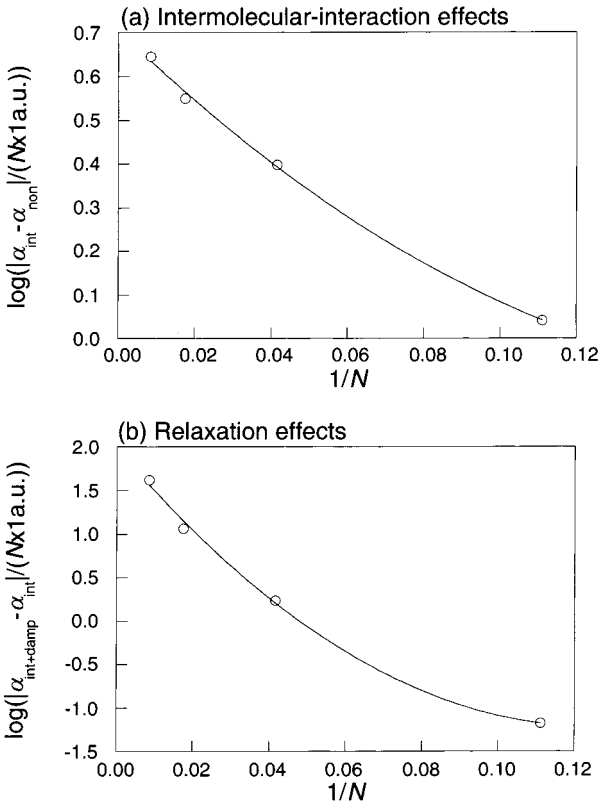

Figure 3. Size-dependency of intermolecular-interaction effects (log-($|\alpha_{int} - \alpha_{non}|/(N \times 1$ au)) vs $1/N$) (a) and the damping effects (log-($|\alpha_{int+damp} - \alpha_{int}|/(N \times 1$ au)) vs $1/N$) (b). N represents the number of monomers. It is noted that $\alpha_{int} - \alpha_{non}$ values are positive, whereas $\alpha_{int+damp} - \alpha_{int}$ values are negative in sign. $(\alpha_{int} - \alpha_{non})/N$ values for D10, D25, D58, and D127 are 1.100, 2.504, 3.546, and 4.418 au, respectively, whereas $(\alpha_{int+damp} - \alpha_{int})/N$ values for D10, D25, D58, and D127 are −0.066 67, −1.742, −11.62, and −41.93 au, respectively.

Namely, all of the virtual excitation contributions are positive and are more enhanced in the case of smaller transition energies and larger magnitudes of the transition dipole $|\mu_{1l}|$.

In the present case (off-resonant α of systems with weak intermolecular interactions), the total α value is found to almost linearly enhance with the increase in the number of monomers. This feature indicates that the magnitude of off-resonant α for the present systems is primarily determined by the number of monomers and their relative configurations with respect to the applied field. Therefore, we confine our attention to the intermolecular-interaction and damping effects on α. The α value including only intermolecular-interaction effects is referred to as α_{int}; the α value including both intermolecular interaction and damping effects is referred to as $\alpha_{int+damp}$. The α value including neither effects is referred to as α_{non}. The monomer value of α_{non} is 89.97 au. Figure 3 parts a and b show the size dependences of intermolecular-interaction ($\alpha_{int} - \alpha_{non}$) and damping ($\alpha_{int+damp} - \alpha_{int}$) effects on α per unit dipole for these aggregate models, respectively. It is found that the intermolecular-interaction and damping effects provide positive and negative contributions to α, respectively (see the legend of Figure 3). In accordance with the fitting procedure in previous studies,[18,19] Δα ($= \alpha_{int} - \alpha_{non}$ or $\alpha_{int+damp} - \alpha_{int}$) per unit dipole is fitted by the least squares to

$$\log\left(\frac{|\Delta\alpha|}{N}\right) = p + \frac{q}{N} + \frac{r}{N^2} \qquad (16)$$

where the extrapolated values for infinite N are $(|\Delta\alpha|/N)_{N\to\infty} =$

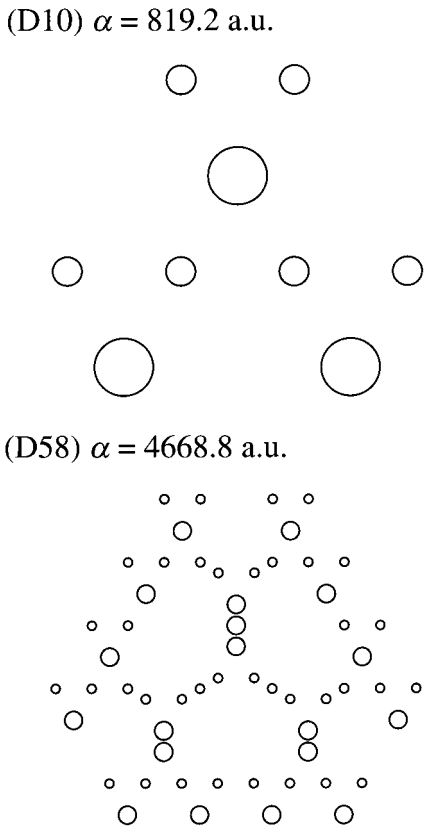

Figure 4. Calculated α ($= \alpha_{xx}$) [a.u.] and its partitioned $\alpha_{|1,1,...,1\rangle-b}$ (spatial contribution) for the dendritic aggregates D10 and D58 (Figure 1) involving intermolecular interactions and damping effects. The size of the circle at each dipole site represents the magnitude of $\alpha_{|1,1,...,1\rangle-b}$. The scale factors of these systems are different from each other. The symbol *b* indicates a one-exciton aggregate basis (see eq 14). These α values are the same as those for $\alpha_{int+damp}$ in section 3.1.

TABLE 1: Fitting Parameters *p*, *q*, and *r* in Equation 16 for the Intermolecular-Interaction ($\alpha_{int} - \alpha_{non}$) and Damping ($\alpha_{int+damp} - \alpha_{int}$) Effects in Dendritic Aggregates from D10 to D127 Shown in Figure 1

	p	*q*	*r*
intermolecular-interaction effect	0.7056	−8.412	21.95
damping effect	1.988	−51.22	205.0

10^p. The fitting parameters *p*, *q*, and *r* are listed in Table 1. In this plot, we use the data from D10 to D127, whereas the data for D4 are not used because D4 possesses only one generation and exhibits a distinct feature of structure compared with other dendritic aggregates composed of multigenerations. It is noted that the present planar dendritic aggregates with Cayley-tree structures over D127 hardly seem to exist because of the steric hindrance of dendron parts in the periphery region. Actually, the Cayley-tree-type planar dendrimers over D127 have not been synthesized.[9] Even though such extended systems exist, they will take nonplanar structures, which do not conform to the models considered in this study. The nonlinear size-dependency of $(\alpha_{int} - \alpha_{non})/N$ suggests that the intermolecular-interaction effects on transition energies and moments nonlinearly depend on the number of monomers in linear leg regions parallel to the polarization vector of the applied field. Because it is well-known that the *J*-aggregate-type interaction decreases the dipole-allowed excitation energies, the size dependence of the intermolecular-interaction effect on α is predicted to be determined by the number of *J*-aggregate-type interaction pairs involved in linear leg regions in each model. For large-size aggregates,

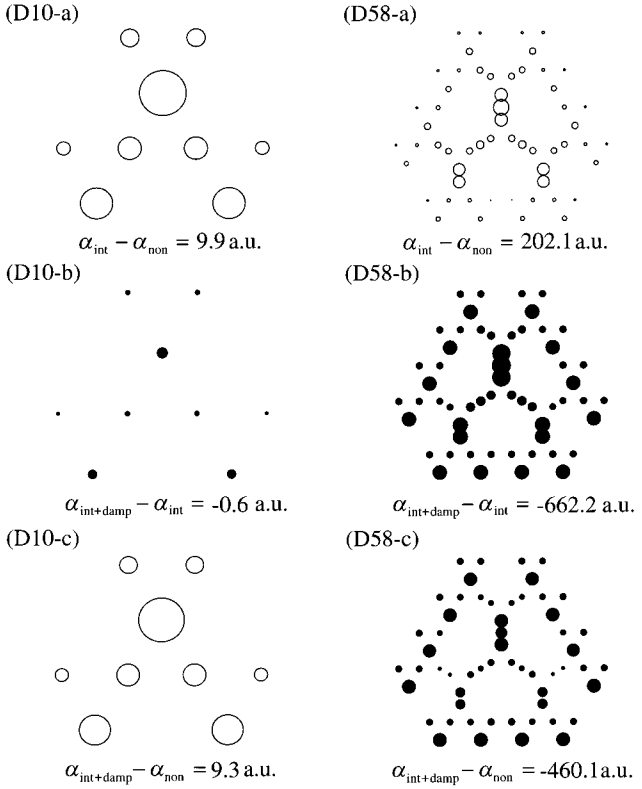

Figure 5. Differences shown iby D10-a and D58-a: $\alpha_{int} - \alpha_{non}$ (see section 3.1 for the notation of α) of D10 and D58 (Figure 1), respectively. Damping effects in one-exciton states are omitted in these cases. Differences shown by D10-b and D58-b: $\alpha_{int+damp} - \alpha_{int}$ of D10 and D58, respectively (Figure 1). Total effects shown by D10-c and D58-c: $\alpha_{int+damp} - \alpha_{non}$ of D10 and D58, respectively. It is noted that D10 takes a nonfractal structure, whereas D58 does a fractal structure. The white and black circles represent positive and negative contributions, respectively, and the size of the circle indicates the magnitude of the contribution. The scale factors of circles for these systems are different from each other.

the damping effects (negative contribution) are found to overcome the intermolecular-interaction effects (positive contribution), so that the total α values for large-size dendritic aggregates tend to slightly decrease.

The spatial one-exciton contributions to the off-resonant α for D10 (nonfractal structure) and D58 (fractal structure) are shown in Figure 4. All of the contributions are found to be positive in sign, as is expected from eq 15. In agreement with our prediction, the dominant contributions for both systems are shown to be distributed in linear leg regions parallel to the polarization vector of the applied field. This feature can be understood by the fact that these linear leg regions possess a dominant interaction with the applied field because their dipole units are parallel to the polarization vector of applied field.

3.2. Effects of Intermolecular Interaction and Damping on the Spatial Contribution of One-Exciton Generation to α. First, we only focus on the effects of intermolecular interaction on α, so that the damping terms are omitted. Figure 5. parts D10-a and D58-a show the effects of the intermolecular interaction on the one-exciton generation contributions to α. For both systems, the total α values are found to be slightly enhanced by the intermolecular interaction compared to that of α_{non}, respectively. The dominantly enhanced contributions of one-exciton generation are shown to be located in the linear leg regions parallel to the polarization vector of the applied field. Although the contributions in these linear leg regions of both systems are found to be different among generations, D10 shows

much smaller variation than D58 (for example, compare regions **a** and **e**(**e**′) in D10 with regions **a**, **e**(**e**′), and **f**(**f**′) in D58). This feature relates to the fact that D10 possesses a smaller number of monomers in its linear legs (only one monomer per each liner leg) compared to D58. For D58, the contributions in inner leg regions are distinctly larger than those in outer leg regions: **a** > **e**(**e**′) > **f**(**f**′) and **h**(**h**′) > **g**(**g**′) > **i**(**i**′), **j**(**j**′), and **k**(**k**′). Namely, the inner linear leg regions for D58 primarily contribute to lower one-exciton energy states because of their larger number of *J*-aggregate-type pairs as compared to outer leg regions. Such differences in the spatial contributions to α between D10 and D58 reflect their architectures, i.e., fractal and nonfractal structures, because the number of monomers in leg regions for the fractal architecture increases as going from the periphery to the core.

Next, we consider the damping effects in one-exciton states on α. In contrast to the intermolecular-interaction effects, the contributions (negative in sign) occur significantly both in inner and in outer linear leg regions. It is also found that the damping effects in a large-size aggregate (D58) remarkably reduce the $\alpha_{int+damp}$ compared to those in a small-size aggregate (D10). From our introducing way of damping terms, these reductions are presumed to originate in the decoherence process, i.e., the decrease in the off-diagonal density matrixes, because of the phase damping effects (see eqs 7 and 9).

Although the total effects (intermolecular-interaction and damping effects) for D10 are found to slightly enhance α, those for D58 are found to reduce α (see Figure 5 parts D10-c and D58-c). This feature implies that the damping effects (negative contribution) are more significant for larger-size dendritic aggregates because larger-size aggregates possess larger multistep energy widths which lead to larger damping factors.

4. Concluding Remarks

In this study, we investigated the off-resonant α for several sizes of model dendritic aggregates (D4, D10, D25, D58, and D127) with planar structures and elucidated the features of spatial contributions of one-exciton generation to α for fractal and nonfractal dendritic aggregate systems. It was found that the size dependence of intermolecular-interaction enhancement of α/N is nonlinear and is closely related to the number of *J*-aggregate-type-interaction pairs involved in each system. The intermolecular interaction and the damping in one-exciton states were shown to provide slight effects with mutually opposite sign on α: the former enhances the α, whereas the latter reduces that. The α values of the present fractal dendritic systems were found to be dominantly contributed to by the one-exciton generation distributed in linear leg regions, especially the central leg region, parallel to the polarization vector of applied field, whereas for nonfractal dendritic systems, the dominant intermolecular-interaction contribution in each generation showed slight differences among generations. This feature can be understood by the fact that the fractal structure provides a larger number of *J*-aggregate-type-interaction pairs, which leads to the decrease in the one-exciton energies, as going from the periphery to the core in contrast to the nonfractal structure. In contrast to these intermolecular-interaction effects, the damping effects were shown to provide mutually similar contributions both in inner and in outer linear leg regions for these systems. The reduction of α by the damping effects is presumed to be caused by the phase damping effects. In the present cases, the reduction of α was more significantly observed in larger-size aggregates than in smaller-size aggregates.

On the analogy of the present results, the fractal supramolecular systems with electronically well decoupled generations are predicted to possess an attracting feature: the contribution of one-exciton generation to α varies for each generation from the periphery to the core. This feature is expected to be observed as a more remarkable and more complicated phenomena in the (near)resonant high-order response processes, e.g., hyperpolarization under intense laser field. The efficiency of the calculation and analysis approach presented in this study will be displayed better in the case of treating such phenomena.

Finally, we make some suggestions on the experimental realization of these attracting features. The measurements of α for the several aggregates (with different intermolecular interactions) arranged artificially on the surface may be possible. Also, as mentioned above, the size dependences of α and hyperpolarizabilities for several sizes of supramolecular systems (dendrimers) are expected to more remarkably reflect the effects of the fractal structure. For example, the size dependences of α and hyperpolarizabilities for three types of phenylacetylene oligomers, (*para*-connencted, nonfractal-structured *meta*-connected, and fractal-structured *meta*-connected (which is actually involved in phenylacetylene dendrimers) oligomers) are expected to be remarkably different from each other. The theoretical investigations of these species are now in progress in our laboratory.

Acknowledgment. This work was supported by a Grant-in-Aid for Scientific Research on Priority Areas (No. 12042248, 12740320, and 10149105) from the Ministry of Education, Culture, Sports, Science and Technology, Japan.

References and Notes

(1) Knox, R. S. *Primary Processes of Photosynthesis*; Barber, J., Ed.; Elsevier: Amsterdam, The Netherlands, 1977, 55.
(2) Pope, M.; Swenberg, C. E. *Electronic Processes in Organic Crystals*; Oxford University Press: Oxford, U.K., 1982.
(3) Webber, S. E. *Chem. Rev.* **1990**, *90*, 1469.
(4) Tomalia, D. A.; Naylor, A. M.; Goddard, W. A. *Angew. Chem., Int. Ed. Engl.* **1990**, *29*, 138.
(5) Jiang, D.-L.; Aida, T. *Nature* **1997**, *388*, 454.
(6) Mukamel, S. *Nature* **1997**, *388*, 425.
(7) Fox, M. A.; Jones, W. E.; Watkins, D. M. *Chem. Emg. News* **1993**, *119*, 6197.
(8) Devadoss, C.; Bharathi, P.; Moore, J. S. *J. Am. Chem. Soc.* **1996**, *118*, 9635.
(9) Shortreed, M. R.; Swallen, S. F.; Shi, Z.-Y.; Tan, W.; Xu, Z.; Devadoss, C.; Moore, J. S.; Kopelman, R. *J. Phys. Chem. B* **1997**, *101*, 6318.
(10) Kopelman, R.; Shortreed, M.; Shi, Z.-Y.; Tan, W.; Bar-Haim, A.; Klafter, J. *Phys. Rev. Lett.* **1997**, *78*, 1239.
(11) Bar-Haim, A.; Klafter, J.; Kopelman, R. *J. Am. Chem. Soc.* **1997**, *119*, 66197.
(12) Tretiak, S.; Chernyak, V.; Mukamel, S. *J. Phys. Chem. B* **1998**, *102*, 3310.
(13) Nakano, M.; Takahata, M.; Fujita, H.; Kiribayashi, S.; Yamaguchi, K. *Chem. Phys. Lett.* **2000**, *323*, 249.
(14) Nakano, M.; Yamaguchi, K. *Phys. Rev. A* **1994**, *50*, 2989.
(15) Harigaya, H. *Int. J. Mod. Phys. B* **1999**, *13*, 2631; *Phys. Chem. Chem. Phys.* **1999**, *1*, 1687.
(16) Spano, F. C.; Knoester, J. *Adv. Magn. Opt. Res.* **1994**, *18*, 117.
(17) Spano, F. C.; Kuklinski, J. R.; Mukamel, S. *Phys. Rev. Lett.* **1990**, *65*, 211.
(18) Hurst, G. J.; Dupuis, M. *Chem. Phys. Lett.* **1990**, *171*, 201.
(19) Nakano, M.; Shigemoto, I.; Yamada, S.; Yamaguchi, K. *J. Chem. Phys.* **1995**, *103*, 4175.